

# A Search for Higgs Boson in $H \rightarrow W^+W^-$

Kevin Sung on behalf of the CMS Collaboration  
Massachusetts Institute of Technology, Cambridge, MA, USA

A search for the Higgs boson decaying to  $W^+W^-$  has been performed on  $1.1 \text{ fb}^{-1}$  of pp collision data at  $\sqrt{s} = 7 \text{ TeV}$  collected with the Compact Muon Solenoid (CMS) detector in 2011. No significant excess above Standard Model background expectation is observed, and upper limits on Higgs boson cross section production are derived, excluding the presence of a Higgs boson with mass in the range of  $[150, 193] \text{ GeV}/c^2$  at 95% confidence level.

## 1. Introduction

The Standard Model (SM) of particle physics successfully explains the majority of high-energy experimental data [1]. One of the key remaining questions is the origin of masses of elementary particles. In the SM, it is attributed to spontaneous breaking of the electroweak symmetry [2–4]. The existence of the field quantum, the Higgs boson, has still to be experimentally confirmed.

The first search for the Higgs boson at the LHC was published by CMS based on a data sample recorded in 2010 using the fully leptonic final state [5]. The strategy adopted in [5] has been improved to cope with a larger number of interactions within a single bunch crossing, referred to as *pile-up*. Furthermore, to improve signal sensitivity, lower transverse momentum ( $p_T$ ) and events with one and two reconstructed jets are now considered. The analysis is performed using an integrated luminosity of  $1.1 \pm 0.1 \text{ fb}^{-1}$  [6].

The analysis separates the full set of  $H \rightarrow WW \rightarrow \ell\nu\ell'\nu'$  events into three categories according to the event jet multiplicity:  $H + 0$  jets,  $H + 1$  jet, and  $H + 2$  jets.  $W^+W^-$  candidates with both  $W$  bosons decaying leptonically are selected in final states consisting of two isolated, high  $p_T$ , oppositely charged leptons (electrons or muons) and large missing transverse energy due to the undetected neutrinos. The search for the Higgs boson is performed in the mass range of  $115 - 600 \text{ GeV}/c^2$ , using both a cut-based signal extraction and a multivariate analysis. All Higgs production mechanisms are considered as part of the signal: the gluon fusion process, a Higgs boson in the final state accompanied by a  $W$  or  $Z$  boson or by a pair of top quarks, and the vector boson fusion (VBF) process. The latter process plays a major role in the 2-jet category. The expected production cross sections for a SM Higgs boson are taken from [7].

## 2. Event Preselection

Several SM processes can lead to a final state similar to that of  $H \rightarrow W^+W^-$  signal, in addition to the non-resonant  $W^+W^-$  process. These backgrounds include:  $W$ +jets and QCD multi-jet events where at least one of the jets is misidentified as a lepton, top production ( $t\bar{t}$  and  $Wt$ ), the Drell-Yan  $Z/\gamma^* \rightarrow \ell^+\ell^-$  process, and diboson production ( $W\gamma$ ,  $WZ$ ,  $ZZ$ ).

Events are selected with two oppositely charged, isolated leptons with high transverse momenta ( $p_T$ ), in three final states:  $e^+e^-$ ,  $\mu^+\mu^-$ , and  $e^\pm\mu^\mp$ . These final states include  $W \rightarrow \tau\nu_\tau$  events with leptonic  $\tau$  decays. The trigger system requires the presence of one or two high  $p_T$  leptons. The trigger efficiency for signal events is found to be above 97% in the  $\mu^+\mu^-$  final state and above 99% in the  $e^+e^-$  and  $e^\pm\mu^\mp$  final states for a Higgs boson with  $m_H \sim 160 \text{ GeV}/c^2$ .

Charged leptons from  $W$  boson decays are expected to be isolated from other activity in the event. For each lepton candidate, a cone of radius  $\Delta R \equiv \sqrt{\Delta\eta^2 + \Delta\phi^2} < 0.3$  (0.4) for muons (electrons) is constructed around the track direction at the event vertex. The scalar sum of the transverse energy of charged particle candidates [8] compatible with the chosen primary vertex and contained within the cone is calculated, excluding the contribution from the lepton candidate itself. If this sum exceeds some fraction of the candidate  $p_T$ , the lepton is rejected. The exact requirement depends on lepton  $\eta$ ,  $p_T$ , and flavor.

Neutrinos from  $W$  boson decays escape detection. This results in an imbalance in the measured energy depositions in the transverse plane, denoted by  $E_T^{\text{miss}}$ . To reject  $Z/\gamma^* \rightarrow \tau^+\tau^-$  background events as well as  $Z/\gamma^* \rightarrow \ell^+\ell^-$  events with mis-measured  $E_T^{\text{miss}}$  associated with poorly reconstructed leptons, we use the *projected*  $E_T^{\text{miss}}$  [9]. This is calculated as the component of  $E_T^{\text{miss}}$  transverse to the closest lepton if it is closer than  $\pi/2$  in azimuthal angle, and the full  $E_T^{\text{miss}}$  otherwise. To reduce the dependence of the *projected*  $E_T^{\text{miss}}$  on pile-up we use the minimum of two different estimators: the first includes all particle candidates in the event [10], while the

second uses only the charged particle candidates associated to the primary vertex. This exploits the correlation between the two estimators in events with real *projected*  $E_T^{\text{miss}}$ , as in the signal, and uncorrelation otherwise, as in Drell-Yan events. Events are required to have *projected*  $E_T^{\text{miss}}$  above 40 GeV in the  $e^+e^-$  and  $\mu^+\mu^-$  final states, and above 20 GeV for the  $e^\pm\mu^\mp$  final states, which have lower contamination from  $Z/\gamma^* \rightarrow \ell^+\ell^-$  decays. To reduce the contamination from  $Z/\gamma^* \rightarrow \ell^+\ell^-$  events where the  $Z$  boson recoils against a jet, the angle in the transverse plane between the dilepton system and the most energetic jet must be smaller than 165 degrees in the  $ee/\mu\mu$  final states. This selection is only applied if the leading jet  $p_T > 15$  GeV/ $c$ .

To further reduce the Drell-Yan background in the  $ee$  and  $\mu\mu$  final states, events with a dilepton invariant mass within  $\pm 15$  GeV/ $c^2$  of the  $Z$  mass are rejected. Events with dilepton masses below 12 GeV/ $c^2$  are also rejected to suppress contributions from low mass resonances.

Jets are reconstructed from calorimeter and tracker information using the anti- $k_T$  clustering algorithm [11] with distance parameter  $R = 0.5$ . Jets are required to have  $p_T > 30$  GeV/ $c$  within  $|\eta| < 5.0$ . To correct for the pile-up contribution to the jet energy, a method to determine a median energy density per event is applied [12] to compute the offset to be subtracted from the jet  $p_T$  [13].

To suppress the top quark background, we apply a *top veto* based on soft-muon and  $b$ -jet tagging [14, 15]. The first method vetoes events containing muons from the  $b$ -quark decays. The second method uses standard  $b$ -jet tagging looking for tracks with large impact parameter within jets. The algorithm is applied also in the case of zero counted jets, which can still contain low  $p_T$  tagged jets.

To reduce the background from diboson processes, such as  $WZ$  and  $ZZ$  production, any event that has an additional third lepton passing the identification and isolation requirements is rejected.  $W\gamma$  production, where the photon is misidentified as an electron, is suppressed by stringent  $\gamma$  conversion rejection requirements. After applying all preselection requirements, 626, 334, 175 events are observed in data coming from 0-jet, 1-jet, and 2-jet categories, respectively. This sample is dominated by  $W^+W^-$  events.

### 3. Higgs Signal Extraction

To enhance the sensitivity to the Higgs signal, two different analyses are performed in the 0-jet and 1-jet categories. The first analysis is a cut-based approach where further requirements on a few observables are applied, while the second analysis makes use of multivariate techniques. Both of them cover a large Higgs boson mass range, and each is separately optimized for different  $m_H$  hypotheses. The first method is the simplest approach to be performed on the recorded data sample. The second method is more powerful, since it exploits the information present in the correlation among the variables. The 2-jet category makes use of a simple cut-based approach for now, since in any case the sensitivity with the current available integrated luminosity is limited.

#### 3.1. Strategy in the 0-jet and 1-jet Categories

In the cut-based approach, extra requirements are placed on the transverse momenta of the harder ( $p_T^{\text{max}}$ ) and softer ( $p_T^{\text{min}}$ ) leptons, the dilepton mass ( $m_{\ell\ell}$ ), the transverse Higgs mass ( $m_T^{\ell\ell E_T^{\text{miss}}}$ ), and the azimuthal angle difference between the two selected leptons ( $\Delta\phi_{\ell\ell}$ ). Figures 1 - 5 show these distributions after preselection, for a SM Higgs signal with  $m_H = 130$  GeV/ $c^2$  and for backgrounds, in the 0-jet and 1-jet categories.

The kinematics of the Higgs boson decay depend on its mass, so the best performance is obtained by optimizing the selection requirements for each value of the mass. The values of the selections were chosen to minimize the upper limit on Higgs cross section, in the hypothesis of no signal. The same cut values are used in the 0-jet and 1-jet categories. In the multivariate approach, a boosted decision tree (BDT) algorithm [16] is used, trained for each Higgs boson mass hypothesis and jet category. In addition to the  $W^+W^-$  selection requirements, a loose cut on the upper value of  $m_{\ell\ell}$  is applied to enhance the signal-to-background ratio. The multivariate technique uses the following additional variables compared to the cut-based analysis:  $\Delta R_{\ell\ell} \equiv \sqrt{\Delta\eta_{\ell\ell}^2 + \Delta\phi_{\ell\ell}^2}$  between the leptons, with  $\Delta\eta_{\ell\ell}$  being the  $\eta$  difference between the leptons, which has similar properties as  $\Delta\phi_{\ell\ell}$ ; the transverse mass of both lepton- $E_T^{\text{miss}}$  pairs; and finally, the lepton flavors. The training is performed using  $H \rightarrow W^+W^-$  as signal and  $W^+W^-$  continuum as background. The BDT outputs for  $m_H = 130$  GeV/ $c^2$  are shown in Figure 6 for 0-jet and 1-jet events. The full distribution of the BDT output is used to compute confidence levels. To enhance the sensitivity to Higgs signal, we use two categories: same-flavor dilepton ( $ee/\mu\mu$ ) events and opposite flavor dilepton ( $e\mu$ ) events.

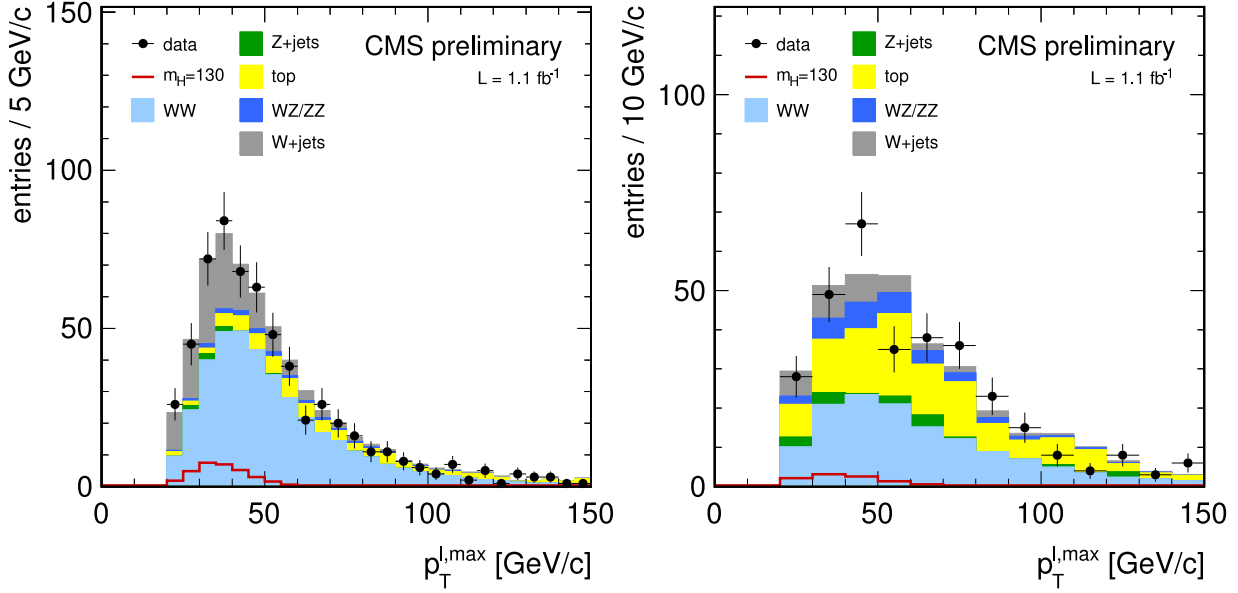


Figure 1: Transverse momentum distributions of the harder lepton for the 0-jet (left) and 1-jet (right) categories.

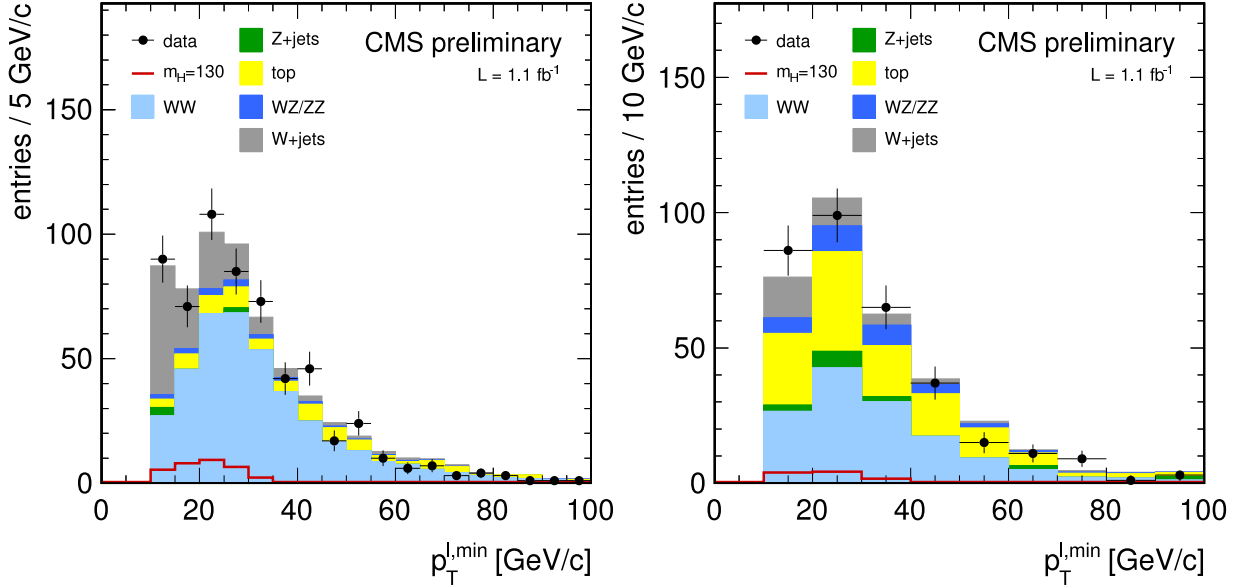


Figure 2: Transverse momentum distributions of the softer lepton for the 0-jet (left) and 1-jet (right) categories.

### 3.2. Strategy in the 2-jet Category

The 2-jet category is mainly sensitive to the VBF production mode. The cross section for this mode is roughly ten times smaller than the gluon-gluon fusion mode. However, the VBF signal can be extracted using simple selections, especially in the fully leptonic decay mode where the backgrounds are expected to be relatively low.

The  $H \rightarrow W^+W^-$  events from VBF production are characterized by a pair of energetic forward-backward jets and very little hadronic activity in the rest of the event. As a starting point, we select events that pass the preselection requiring two reconstructed jets with  $p_T > 30$  GeV/c and no other jets with  $p_T > 30$  GeV/c. To reject the main background from top decays we apply two further improvements on the two jets  $j_1$  and  $j_2$ :  $|\Delta\eta(j_1 - j_2)| > 3.5$  and  $m_{j_1 j_2} > 450$  GeV/c<sup>2</sup>.

To improve the selection efficiency for the low mass Higgs signal we select events with the same  $m_{\ell\ell}$  requirements as the 0-jet and 1-jet strategy. The VBF contribution to the total  $H \rightarrow W^+W^-$  signal in the 2-jet category is found to be about 85% after the full event selection for all the mass hypotheses considered.

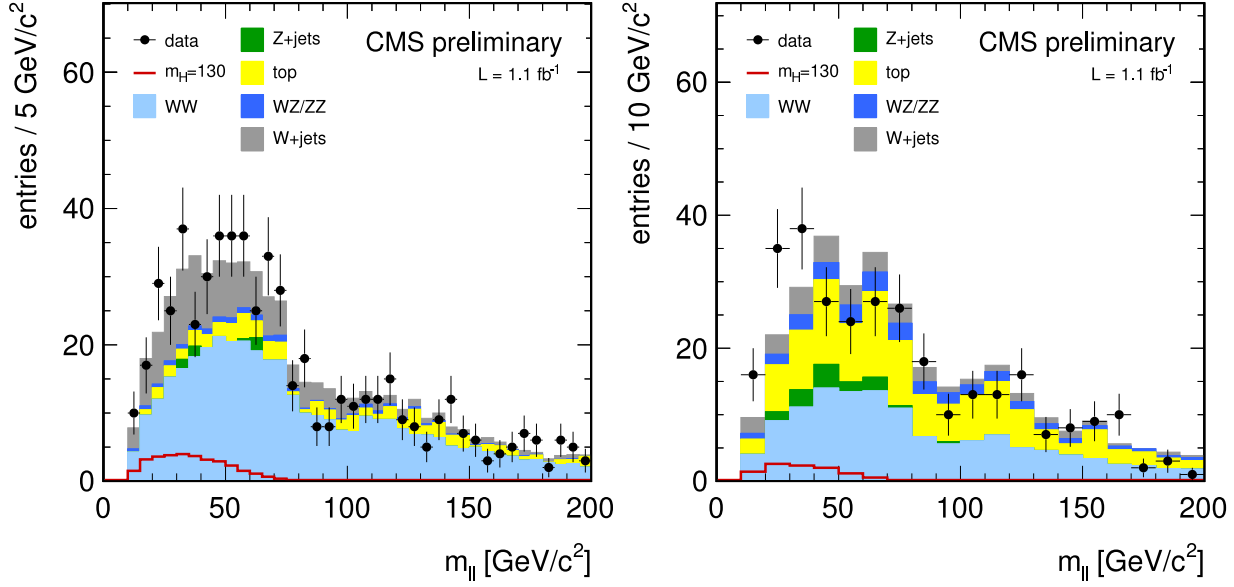


Figure 3: Dilepton mass distributions for the 0-jet (left) and 1-jet (right) categories.

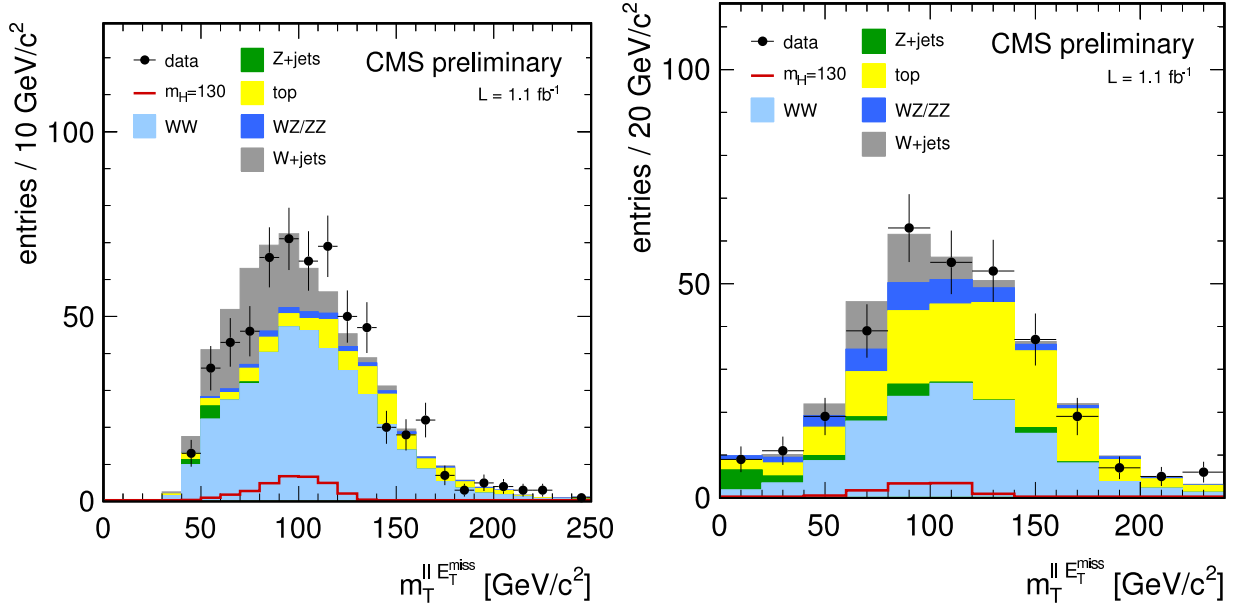


Figure 4: Transverse mass distribution for the 0-jet (left) and 1-jet (right) categories.

#### 4. Background Estimation

Data driven methods are used as much as possible to estimate background contributions to the Higgs signal region. The top background and the  $W$ +jets and QCD multi-jets background are deduced from the measuring the efficiency of particular requirements designed to reject such events and applying the efficiency to a sample of rejected events. The Drell-Yan background in the dielectron and dimuon final states and the non-resonant  $W^+W^-$  background are estimated by scaling the expectation from simulation by a normalization factor between data and simulation in a signal-free control region.

Other backgrounds are estimated from simulation. The  $W\gamma$  background estimate was cross-checked in data using the events passing all selection requirements, except that the two leptons must have the same charge. This sample is dominated by  $W$ +jets and  $W\gamma$  events. For  $WZ$ ,  $ZZ$  and  $Z/\gamma^* \rightarrow \tau^+\tau^-$ , good agreement between the data and the prediction is found.

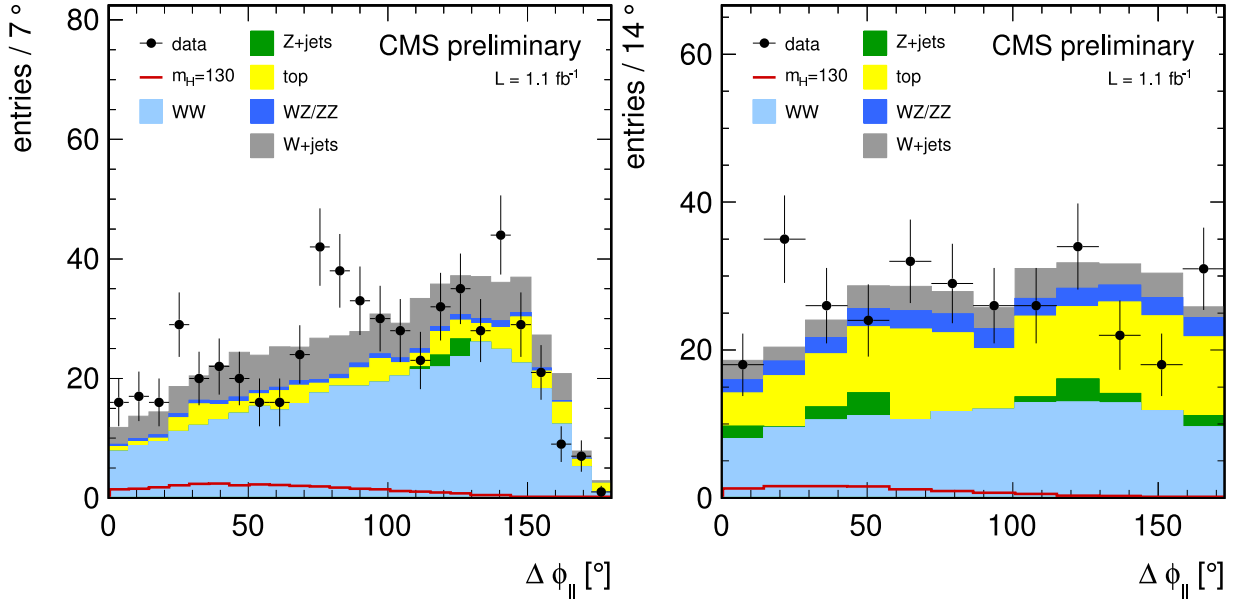


Figure 5: Azimuthal angle difference between the two selected leptons for the 0-jet (left) and 1-jet (right) categories.

#### 4.1. $W$ +jets and QCD multi-jets

$W$ +jets and QCD multi-jet events form a background to  $W^+W^-$  production when jets are misidentified as leptons. The normalization and relevant kinematic distributions are estimated directly from data. A sample of loosely selected lepton candidates is extracted from events dominated by di-jet production. The probability for those candidates to be misidentified as a lepton passing all lepton criteria, referred to as *fake rate*, is calculated. The fake rate is applied to a sample of events selected with the analysis criteria except for one of the leptons for which the selection has been relaxed to the looser criteria and that fails the nominal selection.

#### 4.2. Top

The top background is estimated from data by counting top-tagged events and applying the corresponding tagging efficiency. The tagging efficiency is measured in a data control sample with one counted jet, which is dominated by  $t\bar{t}$  and  $tW$  events. The top-tagging corresponds to the combination of soft-muon and  $b$ -jet tagging.

#### 4.3. Drell-Yan

An estimate of the residual  $Z$  boson contribution to the  $e^+e^-$  and  $\mu^+\mu^-$  final states is obtained by extrapolating the observed number of events in data with dilepton invariant mass within  $\pm 15 \text{ GeV}/c^2$  of the nominal  $Z$  mass. Before performing the extrapolation to the signal region, non-Drell-Yan processes contributing to the control sample must be subtracted. The contribution of  $WZ$  and  $ZZ$  in the  $Z$  mass region, when leptons come from the same  $Z$  boson, is subtracted as estimated from simulation. Other contributions, including  $WW$ , top, and  $WZ$  and  $ZZ$  when both leptons do not come from a  $Z$  boson, are subtracted from an estimate using the  $e^\pm\mu^\mp$  event yield in the  $Z$  mass region, taking into account combinatorics and relative detection efficiencies for electrons and muons.

#### 4.4. $WW$

The non-resonant  $W^+W^-$  contribution in the  $H \rightarrow W^+W^-$  low mass signal region,  $m_H < 200 \text{ GeV}/c^2$ , can be estimated from data. This is done using events with a dilepton mass larger than  $100 \text{ GeV}/c^2$ , where there is a negligible contamination from the Higgs boson signal. For larger Higgs boson masses there is a large overlap between the non-resonant  $W^+W^-$  and Higgs boson signal. In these cases we estimate it from simulation.

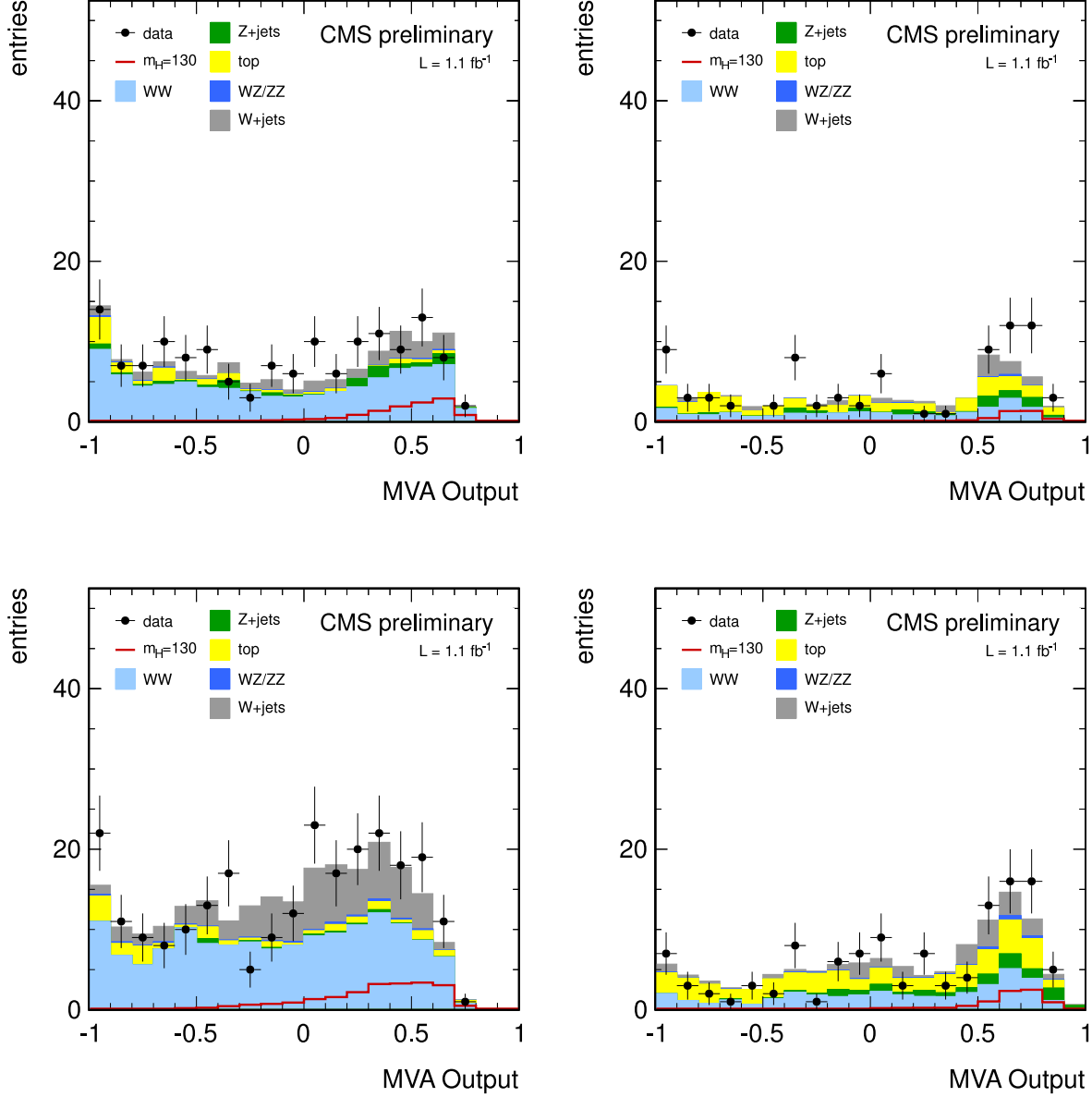


Figure 6: BDT classifier outputs for Higgs signal and background events for  $m_H = 130 \text{ GeV}/c^2$  in the 0-jet bin same flavor final state (top-left), 1-jet bin same flavor final state (top-right), 0-jet bin opposite flavor final state (bottom-left), and 1-jet bin opposite flavor final state (bottom-right), after the  $W^+W^-$  selection. The area marked as  $WW$  corresponds to non-resonant  $W^+W^-$  production.

## 5. Results

The yields after preselection and the expected background contributions are summarized in Table I.

After applying the Higgs mass-dependent selections, no significant excess is found with respect to the expected SM backgrounds, therefore upper limits are derived on the product of the Higgs boson production cross section and the  $H \rightarrow W^+W^-$  branching fraction,  $\sigma_H \times \text{BR}(H \rightarrow W^+W^- \rightarrow \ell\nu\ell'\nu')$ , with respect to the SM expectation,  $(\sigma^{95\%}/\sigma^{SM})$ . The reported results come from a statistical method based on the hybrid Frequentist-Bayesian approach, known as  $CL_S$  [17].

The 95% observed and expected mean C.L. upper limits are shown in Figure 7. Results are reported for both the cut-based and the BDT approach. The bands represent the  $1\sigma$  and  $2\sigma$  probability intervals around

Table I: Expected number of signal and background events from the data-driven methods for an integrated luminosity of  $1.1 \text{ fb}^{-1}$  after applying the  $W^+W^-$  selection requirements. Statistical and systematic uncertainties on the processes are reported. The  $Z/\gamma^* \rightarrow \ell^+\ell^-$  process corresponds to the dimuon and dielectron final states. The  $W^+W^-$  contribution corresponds to the estimated value from the simulation corrected for lepton and trigger efficiencies.

| Process                               | 0-jet            | 1-jet            | 2-jet            |
|---------------------------------------|------------------|------------------|------------------|
| $qq \rightarrow W^+W^-$               | $349.7 \pm 30.3$ | $101.4 \pm 9.3$  | $22.1 \pm 2.0$   |
| $gg \rightarrow W^+W^-$               | $17.2 \pm 1.6$   | $5.9 \pm 0.5$    | $1.1 \pm 0.1$    |
| $t\bar{t} + tW$                       | $63.8 \pm 15.9$  | $141.1 \pm 14.1$ | $99.3 \pm 9.9$   |
| $W + \gamma$                          | $8.7 \pm 1.7$    | $2.4 \pm 0.8$    | $1.1 \pm 0.5$    |
| $WZ + ZZ$                             | $8.5 \pm 0.9$    | $7.2 \pm 0.8$    | $1.5 \pm 0.2$    |
| $Z/\gamma^* \rightarrow \ell^+\ell^-$ | $12.2 \pm 5.3$   | $10.5 \pm 11.5$  | $19.2 \pm 13.5$  |
| $Z/\gamma^* \rightarrow \tau^+\tau^-$ | $1.6 \pm 0.4$    | $10.6 \pm 1.2$   | $3.9 \pm 0.7$    |
| $W + \text{jets}$                     | $106.9 \pm 38.9$ | $36.9 \pm 13.8$  | $16.4 \pm 6.4$   |
| all bkg.                              | $568.6 \pm 52.2$ | $316.0 \pm 24.7$ | $164.6 \pm 18.0$ |
| data                                  | 626              | 334              | 175              |

the expected limit. The a-posteriori probability intervals on the cross section are constrained by the a-priori minimal assumption that the signal and background cross sections are positive definite.

The multivariate analysis is chosen as the reference one because of better Higgs sensitivity. The expected limits for any given mass hypothesis is better by about 30% for the multivariate analysis over the cut-based analysis, and the expected exclusion region is about  $10 \text{ GeV}/c^2$  larger. We exclude the presence of a Higgs boson with a mass in  $[150, 193] \text{ GeV}/c^2$  range at 95% C.L. The observed exclusion range obtained with the cut-based approach is approximately the same. The observed (expected) upper limits are about 0.6 (0.3) times larger than the SM expectation for  $m_H = 160 \text{ GeV}/c^2$ .

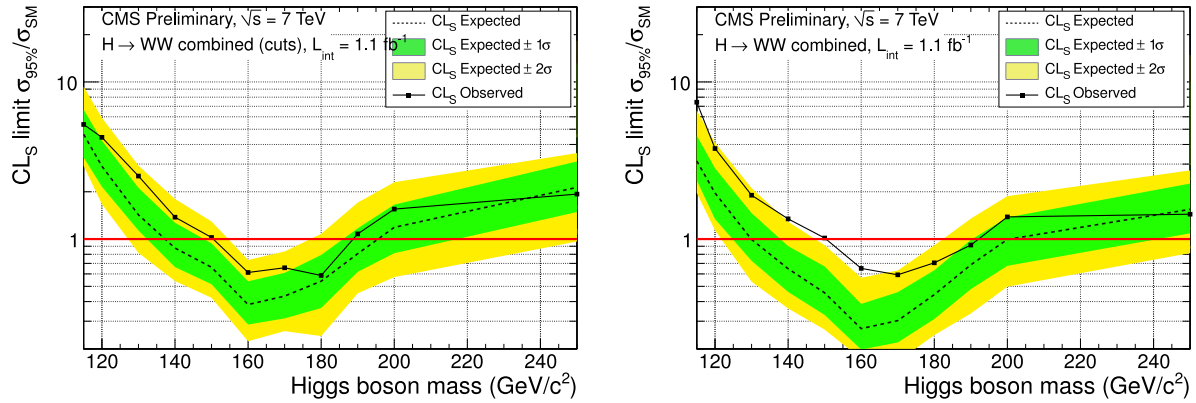


Figure 7: Cut-based (left) and shape-based (right) modified frequentist 95% C.L. expected (dotted line) and observed (points connected by solid line) upper limits on the cross section times branching ratio relative to the SM value.

## 6. Conclusion

A search is performed for the Higgs boson decaying to  $W^+W^-$  in pp collisions at  $\sqrt{s} = 7 \text{ TeV}$ , using a data sample corresponding to an integrated luminosity of  $1.1 \text{ fb}^{-1}$ . No significant excess above the SM background expectation is found, and therefore limits on the Higgs boson production cross section are derived, excluding the presence of a Higgs boson with a mass in  $[150, 193] \text{ GeV}/c^2$  range at 95% C.L.

## References

- 1 K. Nakamura et al.(Particle Data Group), “Review of particle physics”, *J. Phys.* **G37** (2010) 075021. doi:10.1088/0954-3899/37/7A/075021.
- 2 F. Englert and R. Brout, “Broken symmetries and the masses of gauge bosons”, *Phys. Rev. Lett.* **13** (1964) 321. doi:10.1103/PhysRevLett.13.321.
- 3 P.W. Higgs, “Broken symmetry and the mass of gauge vector mesons”, *Phys. Rev. Lett.* **13** (1964) 508. doi:10.1103/PhysRevLett.13.508.
- 4 G. Guralnik, C.Hagan, and T. Kibble, “Global Conservation Laws and Massless Particles”, *Phys. Rev. Lett.* **13** (1964) 585-587. doi:10.1103/PhysRevLett.13.585.
- 5 CMS Collaboration, “Measurement of WW Production and Search for the Higgs Boson in pp Collisions at  $\sqrt{s} = 7\text{TeV}$ ”, \protect\vrule width0pt\protect\href{http://arxiv.org/abs/1102.5429}{arXiv:1102.5429}.
- 6 CMS Collaboration, “Search for the Higgs Boson in the Fully Leptonic  $W^+W^-$  Final State”, *CMS Physics Analysis Summary CMS-PAG-HIG-11-003* (2011).
- 7 LHC Higgs Cross Section Working Group, S. Dittmaier, C. Mariotti et al., “Handbook of LHC Higgs Cross Sections: Inclusive Observables”, \protect\vrule width0pt\protect\href{http://arxiv.org/abs/1101.0593}{arXiv:1101.0593}.
- 8 CMS Collaboration, “Particle Flow Event Reconstruction in CMS and Performance for Jets, Taus, and MET”, *CMS Physics Analysis Summary CMS-PAS-PFT-09-001* (2009).
- 9 CDF Collaboration, “Measurement of the  $W^+W^-$  production cross section and search for anomalous  $WW\gamma$  and  $WWZ$  couplings in  $p\bar{p}$  collisions at  $\sqrt{s} = 1.96\text{ TeV}$ ”, *Phys. Rev. Lett.* **104** (2010) 201801. doi:10.1103/PhysRevLett.104.201801.
- 10 CMS Collaboration, “Commissioning of the Particle-Flow reconstruction in Minimum-Bias and Jet Events from pp Collisions at 7 TeV”, *CMS Physics Analysis Summary CMS-PAS-PFT-10-002* (2010).
- 11 M. Cacciari, G.P. Salam, and G. Soyez, “The anti- $k_t$  jet clustering algorithm”, *JHEP* **04** (2008) 063, \protect\vrule width0pt\protect\href{http://arxiv.org/abs/0802.1189}{arXiv:0802.1189}.
- 12 M. Cacciari and G.P. Salam, “Dispelling the  $N^3$  myth for the  $k_t$  jet-finder”, *Phys. Lett.* **B641** (2006) 57-61, \protect\vrule width0pt\protect\href{http://arxiv.org/abs/hep-ph/0512210}{arXiv:hep-ph/0512210}. doi:10.1016/j.physletb.2006.08.037.
- 13 M. Cacciari and G.P. Salam, “Pileup subtraction using jet areas”, *Phys. Lett* **B659** (2008) 119-126, \protect\vrule width0pt\protect\href{http://arxiv.org/abs/0707.1378}{arXiv:0707.1378}. doi:10.1016/j.physletb.2007.09.077.
- 14 CMS Collaboration, “Algorithms for b-jet identification in CMS”, *CMS Physics Analysis Summary CMS-PAS-BTV-09-001* (2009).
- 15 CMS Collaboration, “Commissioning of b-jet identification with pp collisions at  $\sqrt{s} = 7\text{ TeV}$ ”, *CMS Physics Analysis Summary CMS-PAS-BTV-10-001* (2010).
- 16 A. Hoecker et al., “TMVA - toolkit for multivariate data analysis”, arXiv:0703039.
- 17 R.D. Cousins and V.L. Highland, “Incorporating systematic uncertainties into an upper limit”, *Nucl. Instrum. Meth.* **A320** (1992) 331. Revised version. doi:10.1016/0168-9002(92)90794-5.